

Glioma C6: A Novel Dataset for Training and Benchmarking Cell Segmentation

Roman Malashin^{1,2}, Svetlana Pashkevich³, Daniil Ilyukhin¹, Arseniy Volkov³, Valeria Yachnaya¹, Andrey Denisov³, and Maria Mikhalkova¹

¹Pavlov Institute of Physiology, Russian academy of science

²Saint-Petersburg State University of Aerospace Instrumentation, Russia

³Institute of Physiology, NAS of Belarus

Abstract

We present Glioma C6, a new open dataset for instance segmentation of glioma C6 cells, designed as both a benchmark and a training resource for deep learning models. The dataset comprises 75 high-resolution phase-contrast microscopy images with over 12,000 annotated cells, providing a realistic testbed for biomedical image analysis. It includes soma annotations and morphological cell categorization provided by biologists. Additional categorization of cells, based on morphology, aims to enhance the utilization of image data for cancer cell research. Glioma C6 consists of two parts: the first is curated with controlled parameters for benchmarking, while the second supports generalization testing under varying conditions. We evaluate the performance of several generalist segmentation models, highlighting their limitations on our dataset. Our experiments demonstrate that training on Glioma C6 significantly enhances segmentation performance, reinforcing its value for developing robust and generalizable models. The dataset is publicly available for researchers.

1 Introduction

Deep learning has proven to be effective in aiding cancer cell detection in biopsy-derived tissue samples[1, 2, 3, 4, 5], and the primary focus of our study is *in vitro* tumor cell cultures that offer a complementary avenue for cancer research[6, 7, 8].

Particularly, we are interested in label-free cell detection and analysis methods[9, 10, 11, 12], which provide an alternative to fluorescent labeling. Fluorescent labeling — a widely adopted technique for cancer cell detection in microscopy[13] — involves staining cells with specific fluorescent dyes or genetically encoded markers. This process requires complex sample preparation and specialized imaging equipment. Moreover, it is constrained by photobleaching, variability in staining efficiency, and the fact that it typically necessitates the use of fixed (non-viable) cells, limiting its applicability for long-term or live-cell studies. In our work, we focus on phase-contrast microscopy, a technique commonly used for label-free imaging of *in vitro* cell cultures. However, compared to fluorescence microscopy, it produces lower-contrast images and introduces specific artifacts[16],

making image analysis more challenging. In this context, deep learning plays a crucial role in enabling accurate and robust analysis.

We also address another key aspect of cancer research and drug screening[14, 15]: the analysis of cell morphology, commonly approached through phenotyping, i.e. the characterization of observable features or behaviors. This process includes assessing various cellular attributes, such as shape, proliferation rates and other phenotypic markers. Training deep learning models for such analyses requires datasets with annotated cell shapes, underscoring the need for high-quality labeled data. While numerous datasets exist [19, 20, 17, 21, 22], further expansion is necessary to enhance model robustness and generalization.

In this work, we introduce Glioma C6, a novel annotated dataset of phase-contrast microscopy images of C6 glioma cells, designed to advance cell segmentation research. Unlike many publicly available datasets, we curate a specialized dataset with controlled and consistent parameters, enabling reliable benchmarking in a specialist setting. Additionally, a separate subset of our dataset allows testing generalization under varying conditions.

The Glioma C6 dataset includes over 12,000 annotated cells in total across 75 high-resolution images, with expert annotations distinguishing between two cell types. Additionally, soma annotations are provided for 45 images, captured under consistent shooting conditions.

We summarize our contribution as follows:

- We collect the first open dataset of glioma C6 cells phase-contrast images with soma and cell type annotations.
- Our experiments demonstrate that generalist models still struggle to robustly generalize to new cell datasets without fine-tuning, while fine-tuned models deliver reliable and performance, even under varied imaging conditions (e.g. variations cultivation time).

The dataset is publicly available for research purposes at <https://zenodo.org/records/15083188>.

2 Related works

In this section, we review the most prominent open datasets used in the development of cell segmentation frameworks, along with key deep learning methods for cell segmentation.

Datasets. A variety of datasets have been developed to support the creation of the universal[17] or multimodal cell segmentation models [18]; however, many existing datasets remain limited in diversity, focusing on homogeneous imaging conditions or cell types. The datasets differ along several dimensions, including image resolution, cell types, imaging modalities, and acquisition conditions.

Small-scale datasets typically contain from tens to hundreds of images with tens of thousands of annotated cells. For example, the Cell-APP HeLA dataset consists of 32 images with around 13500 cells [37]. Other examples include DSB 2018[22], which consists of 735 low-resolution images(up to 515×512) of both live cells and fixed specimens, and CellPose[17], which includes 551 images. Dataset [22] was widely used in nuclei detection [40] and segmentation [41, 42, 43, 44, 45] tasks. Medium size datasets contain several thousands of images. For example, LiveCell[19] includes more than 5000 images labeled by professional annotators under the supervision of cell biologists. This dataset was used

in the tasks of the cell center detection [46], cytoplasmic segmentation as well as cell segmentation [47, 48, 49]. OmniPose[21] contains a similar number of images, and only a subset is annotated. This dataset was also used in the task of the cell segmentation [50, 51]. TissueNet is a large-scale dataset [20] comprising over 20,000 images of tissue-derived cells from humans, mice, and macaques. Despite the difference in the number of images, both LiveCell and TissueNet contain a comparable number of annotated cells, each exceeding one million. While several approaches aim to annotate not only cell but also subcellular features, they usually deal with images obtained with fluorescent or electron microscopy techniques [38].

Although Glioma C6 is a comparatively small dataset with approximately 12,000 annotated cells, it stands out due to its unique combination of characteristics.

Methods. In cell segmentation, models designed to generalize across different cell types and image modalities are referred as generalists, while those tailored for specific experimental conditions are called specialists[17, 26]. One of the first successful adaptation of U-Net [?] to universal cell segmentation was CellPose [17] which introduced gradient flows — an output representation that encodes the spatial location of individual cell instances. The same output format was used in MediarFormer [23] — winning solution of multimodality cell segmentation challenge[18]. MediarFormer incorporated Point-wise Attention and Multi-scale Fusion Attention Block[27], test-time augmentation and model ensembles. Recent, CellPose-3 [26] concentrates on enhancing generalist model by accounting different image degradation processes.

A further step forward is the development of foundational models for medical image analysis[28, ?]. For this purpose authors of [24] develop dataset with 1.5m image-mask pairs. They introduced a promptable model, that allows users to specify segmentation targets using bounding boxes. The authors of [29] concentrate on developing foundation model specifically for cell segmentation.

While foundation models represent a promising area, variability in task definitions and imaging modalities complicates the design of fully automatic solutions. Pachitariu et al. [30] advocate human-in-the-loop tuning of generalist models, demonstrating that fine-tuning can be label-efficient. More recent works[31, 32, ?] suggest using Segment Anything Model (SAM)[33]. CellSeg1[32] achieves robust results using only one labeled image for fine-tuning: authors highlight that annotation quality is more important than annotation quantity.

In this work, we evaluate various approaches, including generalist cell segmentation models, under both fine-tuning and zero-shot settings.

3 Glioma C6 dataset

We collect the dataset of phase-contrast images of the C6 glioma cell line, which is widely utilized in neuro-oncology research, originating from a rat glial tumor. The C6 cell line is employed to investigate various aspects of glioma biology, including tumor growth, invasion, and potential therapeutic interventions[34]. One of the most important phenomena investigated in cancer cells culture is a proliferation, an increase in the number of cells as a result of cell growth and cell division (mitosis).

The Cell-APP HeLa dataset [37] is aimed for detection of the mitosis state, but it is based on detection of chromatin shape on fluorescently labeled cells. During mitosis, spread cells round up forming a spherically-shaped volume [39]. It leads to variations in

phase-contrast imaging artifacts thus complicating algorithmic analysis[35]. Variations in cell shape (rounded or flattened) also allow one to assess the degree of cell adhesion to a specific culture substrate, estimate influence of specific compounds on the cells state. Taking into account the importance of the tracking the variations of cells shape, we propose classifying glioma cells into morphological subtypes and investigate performance of deep learning methods to detect the subtypes.

3.1 Methodology

The process of collecting Glioma C6 dataset included stages of cultivation, imaging and annotation.

Cultivation. Passaged C6 glial cells (ATCC CCL-107) from the rat *Rattus norvegicus* (ATCC CCL-107) were cultured at a concentration of 2×10^5 cells/mL in flasks containing F-12K medium (Kaighn’s modification of Ham’s F-12, ATCC 30-2004), supplemented with 10% fetal calf serum (Capricorn, NCS-1A) and a 10^{-4} g/mL solution of gentamicin sulfate. The flasks were incubated at 37°C in an incubator set to 5% CO₂.

Imaging. Images were acquired using a BestScope BS-2092 microscope in phase-contrast mode with 10× and 20× objective lenses at 24 or 72 hours after cell suspension seeding. After 24 hours, glioma cells adhered to the Petri dish surface, acquired a specific shape, and began active division.

Overlapped cells The Glioma C6 dataset differs from typical segmentation datasets in one important aspect: it includes overlapping annotations. This was necessary because our goal was to assess the shapes of individual cells. Therefore, during annotation, we allowed one cell mask to overlap with another whenever required.

Annotation procedure. For cells with complex morphology, fully manual segmentation is preferred, as semi-automatic methods often failed to accurately delineate boundaries. We attempted to speedup the annotation process by generating initial annotations using Segment Anything Model[33], OpenCV, and pretrained version of MediarFormer[23]. However, none of these approaches provided meaningful results in annotation and was not adopted in our procedure. Subsequently, we employed MediarFormer, fine-tuned on early version of our dataset, to accelerate soma annotation. The automatically generated results were then refined through manual correction by the annotators.

The annotations were conducted by a team of biologists experienced in cell culture and microscopy. There were three human annotators with more than two years of experience in glioma C6 cells culture. There were several rounds of annotations; after each round, the results were reviewed by a supervisor, and corrections were applied until no visible issues remained. However, due to the frequent occurrence of complex clusters where cells overlap, some unavoidable uncertainty in the annotation persisted even after careful review. In such cases, the most probable annotation was chosen.

3.2 Dataset structure

We annotate cells, somata, and assign each cell to one of two classes. Overall, there are three labels in the Glioma C6 dataset:

I. Cell Type A

Description. These cells correspond to the first phase of growth (early seeding or post-division stage). They are relatively loosely attached to the substrate. At

this stage, cells exhibit an apparent 3D (convex) morphology — their height is comparable to their width and length.

Visual cues. Two main subtypes are observed: spheroid and spindle-shaped.

- Spheroid type A cells appear as small circular structures and typically exhibit a distinct high-contrast halo around the cell border in microscope images, a feature generally absent in type B cells. They also tend to be smaller in area compared to type B.
- Spindle-shaped type A cells maintain a distinct 3D form, but are elongated along one axis and often show characteristic protrusions.

II. Cell Type B

Description. Type B cells typically correspond to the later phase of growth. In this stage, cells firmly attach to the substrate and spread out, so their thickness is much smaller than their width and length.

Visual cues. Type B cells are flattened and show lower contrast. When viewed from above, they often appear irregularly disk-like, but can also be elongated. Their 2D footprint is usually larger than that of type A cells.

III. Soma

Description. Soma contains the nucleus and surrounding cytoplasm, but excludes extended protrusions. It is the compact cell body itself, representing the functional core of the cell.

Visual cues. Soma includes the central, darker part of the cell, with a central region containing a visible nucleus.

The final Glioma C6 dataset consists of two distinct parts:

- **Glioma C6-gen** includes 30 images, acquired under varying imaging and seeding conditions. We used this dataset to test generalization ability of the tuned models.
- **Glioma C6-spec** contains 45 images, acquired under strictly controlled parameters. We used this dataset to train specialist models for controlled experiments.

Both subsets feature high resolution 2592×1944 images, other characteristics of two parts of dataset are presented in the Table 1.

Table 1: Glioma C6 dataset overview.

Part	Cells	Soma	Images	Lens	Time, h	Amount	Labels
gen	3.9K	-	30	10/20	24, 72	Varies	Cell
spec	8.2K	7.8K	45	10	24	Same	Cell A/B, soma

The gen subset was initially used to optimize parameters for the subsequently collected spec subset, ensuring the most informative imaging conditions. Preliminary binary segmentation experiments indicated that preserving image resolution and maintaining consistency in objective lenses significantly improved segmentation accuracy. We include the gen subset as a valuable resource for studying the generalization abilities of specialist models in glioma instance segmentation.

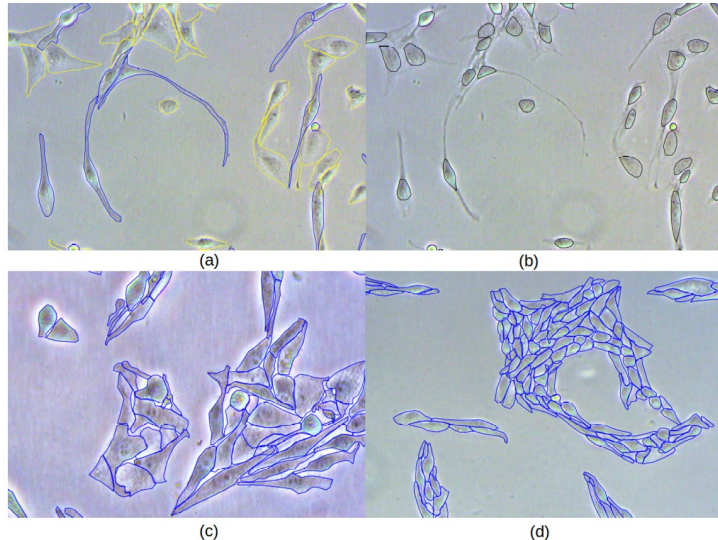


Figure 1: Sample images from the Glioma C6 dataset: (a) **Type A cells** (blue) and **Type B cells** (yellow), (b) **Soma**, (c, d) **Cells from gen subset** captured under varying conditions.

Visual examples of the Glioma C6 dataset are shown in Figure 1, illustrating different cell types and structures.

Similarly to [23] we visualize the shape distribution of Type A and Type B cells through three measures: eccentricity ($\frac{Axis_{short}}{Axis_{long}}$), solidity ($\frac{Area}{Convex Area}$), and cell size (Figure 2).

The figure shows that the mean cell sizes vary across different cell types. Additionally, distribution of eccentricity vs. solidity ratios exhibits distinct patterns, particularly between Type A and Type B cells.

In Figure 2b we present a diagram visualizing the three considered measures for both cell types of Glioma C6.

To facilitate comparison, we extracted subsets from well-known cell segmentation datasets using the same methodology as in [32]:

- 14 subtypes from TissueNet[20].
- Neuronal cells from CellPose[17].
- Blood cells from [28].
- Curated subset from Data Science Bowl (DSB2018) nuclei dataset [22].

The distributions of the characteristics in these datasets are visualized in Figure 3.

As can be seen in Figure 2 and Figure 3 Type A cells possess unique statistics of shape.

4 Experiments

We selected several models for our main experiments: YOLOv11 [36], a widely used general-purpose detector and instance segmentation model; CellPose [26], a well-known generalist model; MediaFormer, an award-winning solution for multimodality cell segmentation [18]; and CellSeg1 [32], a recent low-rank adaptation of the Segment Anything Model tailored for cell segmentation.

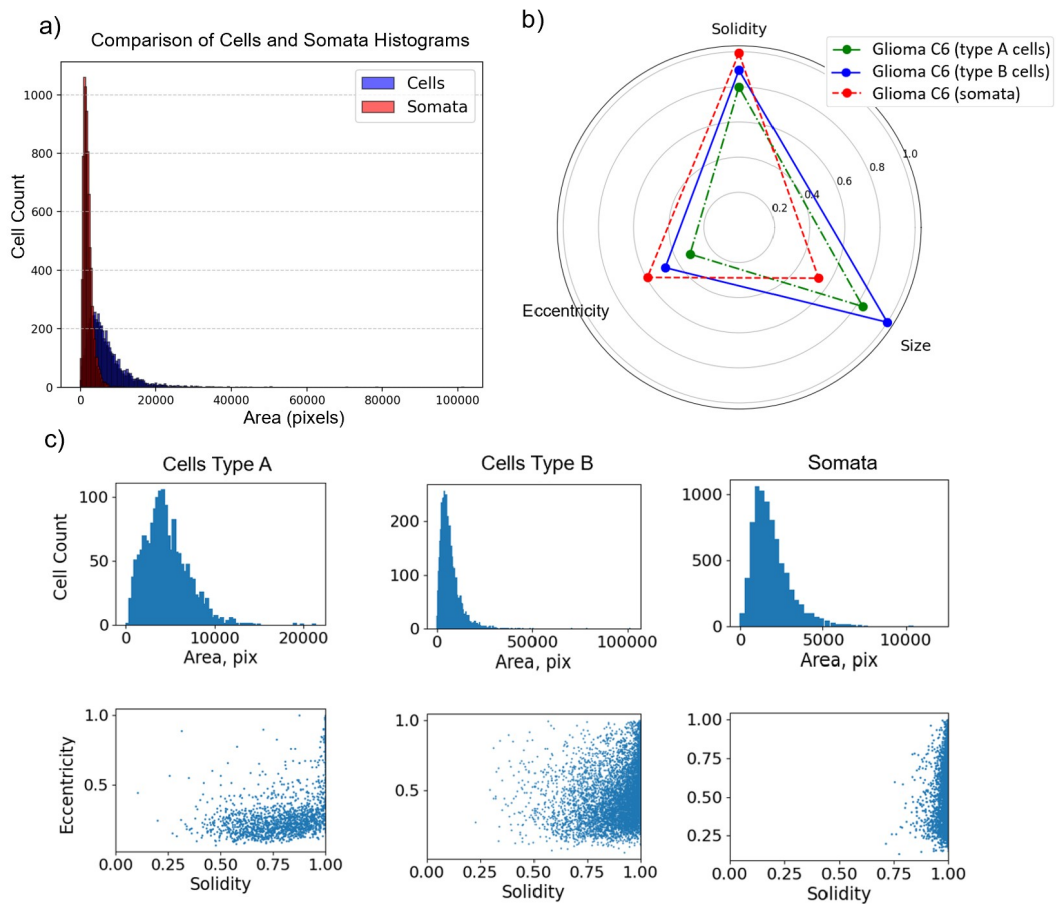


Figure 2: **Shape distribution.** (a) Cell and soma area distribution in spec subset of Glioma C6, (b) Diagram showing eccentricity, solidity and size relation of cells type A and type B and soma, (c) Distribution of solidity vs eccentricity and area for glioma C6 cells and soma.

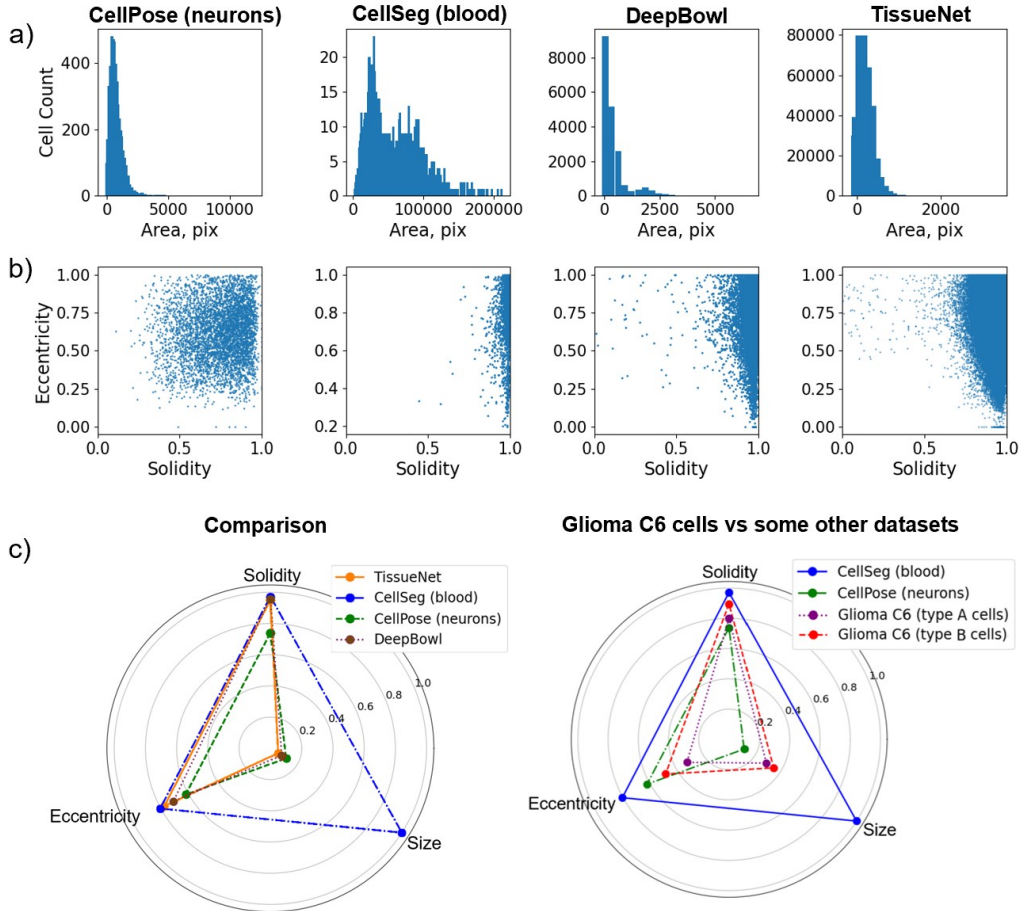


Figure 3: **Datasets statistics.** (a) Distribution of sizes, (b) eccentricity vs. solidity ratio distribution, and (c) Diagram showing relation of mean size, solidity and eccentricity of the cell objects in different datasets

MediarFormer, CellPose, and CellSeg1 are evaluated in both their pretrained form and after fine-tuning on the Glioma C6 dataset (spec part). In the tables the **Glioma-ft** column indicates whether the model was fine-tuned.

Since the cell segmentation models (CellSeg1, MediarFormer, CellPose) cannot be directly applied to multi-class predictions, we trained separate models for instance segmentation of cells (both types), soma, cells type A, cells type B. We used only Glioma C6-spec subset for training.

Metrics. To compare model performance, we use the F1 score at an intersection-over-union (IoU) threshold of 0.5, following [18]. Given the inherent uncertainty in manual cell annotations, an IoU threshold of 0.5 is considered a reasonable criterion for matching. To ensure a more comprehensive evaluation, we additionally report precision, recall, and average precision (AP) (similarly to [17]) at IoU thresholds of 0.5, 0.75, and 0.9. Consistent with [18], cells located at image boundaries are excluded from all evaluations.

Dealing with overlapped cells. Conventional cell segmentation algorithms typically assume that individual cells do not overlap. For instance, diffusion-based approaches employed in CellPose and MediarFormer impose the constraint that each pixel is assigned to exactly one cell. To enable training with such models, we converted the Glioma C6 annotations into binary instance segmentation masks, resolving conflicts deterministically

according to the priority order of the annotated polygons. In contrast, no such conversion was required for YOLOv11, which inherently supports overlapping instances. During validation, all performance metrics in the main paper are reported with respect to the original overlapping annotations. For readers interested in metrics that disregard overlaps (as in the training sets for MediarFormer and Cellpose), we report the corresponding results in Appendix A.

Below, we provide details on training the models.

4.1 Setup

CellSeg1. We trained CellSeg1 for 300 epochs using the parameters suggested by CellSeg1 authors for the dataset [18], which includes resolutions comparable to Glioma C6. The default testing pipeline was suboptimal; however, increasing the number of input crop resolutions — at the expense of processing speed — significantly improved performance, yielding a gain of +0.15 AP@0.5. We also observed high variability in the optimal confidence threshold across training sessions, thus we selected the best value using the validation set. Training on low-resolution images (512×512) used by the authors can be limiting, but increasing this size (without adjusting other parameters) significantly degraded performance. Thus, all the results are reported using these settings.

MediarFormer. The training was conducted for 100 epochs with parameters proposed by the authors of MediarFormer. Weights from phases 1 and 2 after fine-tuning on dataset[18] were used as a starting checkpoint. Training was performed on 512×512 crops. During testing, crops of the same size with a 60% overlap were fed into the network, and the full resolution masks were recovered prior to metrics computation. We report results using an ensemble with Test-Time-Augmentation (TTA), although we did not observe significant performance gains from their usage.

Cellpose. The CellPose cyto3 model[26] was trained for 1000 epochs using the hyperparameters recommended by the authors. The training process incorporated image normalization and augmentation, including random rotations and scaling by a factor of 0.5. During inference images were normalized without any further modifications.

YOLOv11. We used the YOLOv11l (large) model with the default parameters for training and testing. The model was trained for 395 epochs in multi-class regime (with the use of cell and soma class labels), images for training were resized to 1024×1024 . The confidence threshold was kept at the default value of 0.25 during testing.

4.2 Results

We summarize results in Table 2, Figure 4 and Figure 5 provide a visual comparison of the models' predictions.

As expected, YOLOv11 performed poorly, reinforcing the notion that it is not well-suited for cell segmentation tasks. CellSeg1 demonstrates competitive recall, but has significantly lower precision compared to other cell segmentation methods, resulting in reduced overall performance as measured by F1 and AP.

Overall, CellPose achieved the highest performance in both specialist and generalization testing, slightly outperforming MediarFormer. While MediarFormer exhibited higher precision, CellPose attained superior recall. Although performance decreased for all models on the gen subset, it remained stable and sufficiently high across diverse imaging conditions.

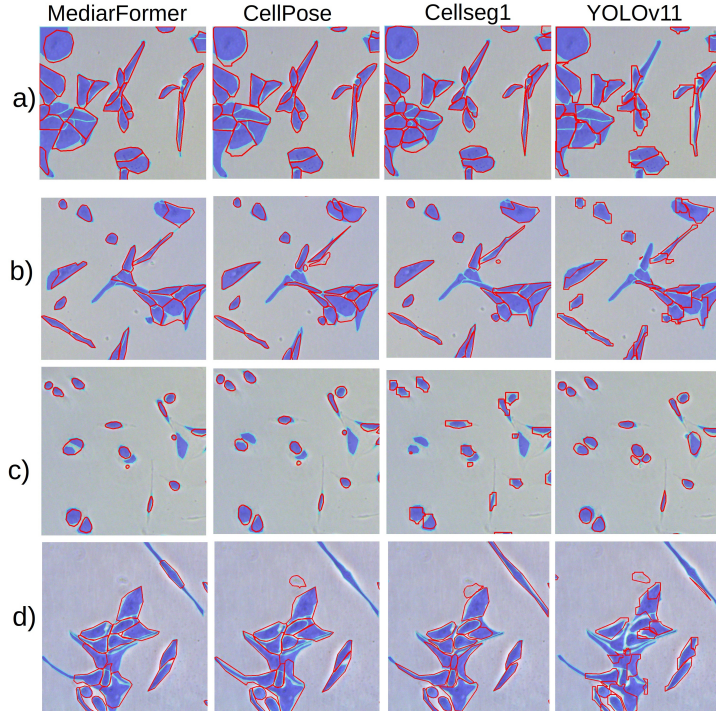


Figure 4: Predictions of the models on the Glioma C6 dataset. Ground truth cell borders are shown in light blue, predictions in red, and binary cell masks in dark blue. (a, b) Cells, (c) somata. Panels (a), (b) and (c) correspond to spec subset, (d) depicts images from the gen subset.

Figure 5 demonstrates models’ predictions on the Glioma C6 dataset for type A and type B cells.

5 Assessment of the annotation uncertainty

Some annotation decisions have inherently unavoidable uncertainty due to the complexity of the annotating clusters of cells. This uncertainty cannot be resolved by human experts relying on the available image data. That means that the same expert can make different annotation decisions based on the same image data. This suggests that the dataset contains inaccuracies, which should limit the maximum AP the ideal algorithm can obtain on Glioma C6 dataset.

In this study, we aim to quantify this uncertainty by performing an independent re-annotation of part of the Glioma C6 dataset. Three experts each independently annotated two images from the Glioma C6 test set. The first image (image 1) was selected as the image with the highest AP@0.5 according to MediarFormer predictions on the original dataset annotation, and the second image (image 2) was selected as the image with the lowest score, where we expect annotation to be particularly challenging. After completing their independent annotations, the experts engaged in a joint review to produce a consensus (consolidated annotation). This consensus annotation was then treated as the reference for comparison against (i) the original Glioma C6 annotation and (ii) CellPose predictions. The comparison results are summarized in Table 3.

The results indicate that the most informative evaluation threshold is AP@0.5. At higher IoU thresholds such as 0.75 and 0.90, the reported values decrease sharply and in

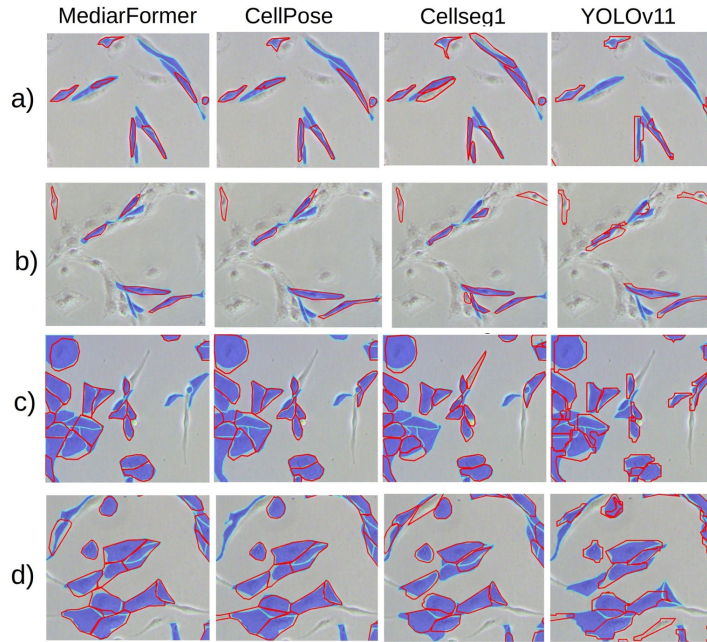


Figure 5: Predictions of the models on the Glioma C6 dataset. (a, b) Type A cells, (c, d) Type B cells. Ground truth cell borders are shown in light blue, predictions in red, and binary binary cell masks in dark blue.

many cases approach zero. This behavior highlights how difficult it is, even for expert annotators, to achieve pixel-accurate agreement on cell boundaries in crowded and low-contrast regions. The qualitative analysis in Figure 6 confirms that, in challenging regions, experts can legitimately disagree on where one cell ends and another begins. Importantly, these discrepancies typically represent plausible alternative segmentations rather than clear annotation mistakes.

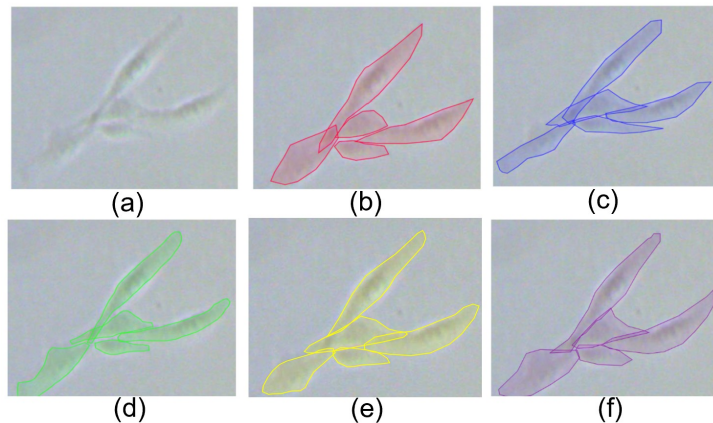


Figure 6: Differences in cell annotations by experts: (a) original image, (b) annotation by the expert-1, (c) annotation by the expert-2, (d) annotation by the expert-3, (e) consolidated annotation by the experts, (f) Glioma C6 dataset annotation.

Furthermore, the subtype-specific scores in Table 3 (cell type A vs. cell type B) show that fine-grained classification of cell subtypes is particularly challenging. The metrics for individual subtypes are consistently lower than those for the combined cell class or

for somata. This suggests that distinguishing between phenotypically similar subtypes is less reliable than detecting “cell vs. background” in general.

The dataset annotation itself shows imperfect agreement with the expert consensus, which indicates that the provided ground truth is not fully self-consistent. This gap likely reflects both the inherent difficulty of tracing boundaries in tightly packed cell clusters and potential annotation fatigue or ambiguity during the original labeling process. Consistent with this interpretation, the Glioma C6 annotation for the image associated with lower MediarFormer scores also exhibits weaker agreement with the expert consensus than the annotation for the image associated with higher MediarFormer scores.

Interestingly, CellPose predictions achieve higher AP scores than the original Glioma C6 annotations when both are evaluated against the expert consensus. This suggests that the model has learned an internally consistent annotation policy and can generate segmentations that are, at least in some cases, more regular and less noisy than the original ground truth. In other words, model training can act as an implicit denoising step: it reduces annotation ambiguity and enforces consistent boundary placement across samples.

Despite these limitations, the Glioma C6 dataset remains highly valuable: it captures realistic, densely packed cellular environments with complex morphology and overlapping structures, i.e. exactly the regimes where automated segmentation is most clinically and biologically relevant. In this sense, the observed disagreement is not a flaw of the dataset itself, but a reflection of the genuine ambiguity of the underlying biological signal.

6 Conclusions

We believe the Glioma C6 dataset serves as a valuable resource for advancing in segmenting and quantifying individual cells within developing dense tumor microenvironments. Accurate instance segmentation of glioma cells enables precise characterization of cell morphology, proliferation patterns, and responses to therapeutic interventions. The dataset introduces unique features that enhance its applicability in specialized studies. In particular, the introduction of two classes of cells based on qualitative features aims to explore the potential of deep learning methods for cell phenotyping, including the potential to detect subtle subcellular variations that are difficult to analyze algorithmically. The results indicate that generalist models exhibit limited generalization to Glioma C6 test images, while fine-tuned models achieve consistent and accurate performance under varied imaging and culturing conditions. This highlights the crucial role of the collected dataset in facilitating model adaptation for glioma segmentation.

7 Acknowledgments

The work was carried out with the financial support of a grant from the St. Petersburg Science Foundation. The study was supported by the State funding allocated to the Pavlov Institute of Physiology, Russian Academy of Sciences (№1021062411653-4-3.1.8). This work was financially supported by BRFFR (SCST) with the grant “Detection of tumor cells in nervous tissue using deep learning methods” (contract No. M24SPbG-010).

References

- [1] Yogesh Kumar, Supriya Shrivastav, Kinny Garg, Nandini Modi, Katarzyna Wiltos, Marcin Woźniak, and Muhammad Fazal Ijaz. Automating cancer diagnosis using advanced deep learning techniques for multi-cancer image classification. *Scientific Reports*, 14(1):25006, 2024.
- [2] I. Hesso et al. Cancer care at the time of the fourth industrial revolution: an insight to healthcare professionals’ perspectives on cancer care and artificial intelligence. *Radiat. Oncol.*, 18(1):167, 2023.
- [3] Ellen N. Huhulea, Lillian Huang, Shirley Eng, Bushra Sumawi, Audrey Huang, Esewi Aifuwa, Rahim Hirani, Raj K. Tiwari, Mill Etienne. Artificial Intelligence Advancements in Oncology: A Review of Current Trends and Future Directions. *Biomedicines*, 13(4):951, 2025.
- [4] X. Jiang, Z. Hu, S. Wang, and Y. Zhang. Deep Learning for Medical Image-Based Cancer Diagnosis. *Cancers (Basel)*, 15(14):3608, July 2023.
- [5] Y. Zhang, S. Wang, X. Liu et al. Biopsy image-based deep learning for predicting pathologic response to neoadjuvant chemotherapy in patients with NSCLC. *npj Precis. Onc.*, 9:132, 2025.
- [6] Magdalena Richter, Oliwia Piwocka, Marika Musielak, Igor Piotrowski, Wiktoria M Suchorska, and Tomasz Trzeciak. From donor to the lab: A fascinating journey of primary cell lines. *Frontiers in Cell and Developmental Biology*, 9:711381, 2021.
- [7] Stefano M. Cirigliano and Howard A. Fine. Bridging the gap between tumor and disease: Innovating cancer and glioma models. *J Exp Med*, 222(1):e20220808, January 6, 2025.
- [8] Nabi Mousavi. Characterization of in vitro 3D cultures. *APMIS*, 129(Suppl 142):1-30, August 2021.
- [9] Shun Wang, Ying Zhou, Xulei Qin, Satish Nair, Xiaohua Huang, and Ying Liu. Label-free detection of rare circulating tumor cells by image analysis and machine learning. *Scientific Reports*, 10(1):12226, 2020.
- [10] Weishu Wu, Yu Zhang, Xiaotian Tan, Yuru Chen, Yuhang Cao, Vaibhav Sahai, Nicole Peterson, Laura Goo, Stacy Fry, Varun Kathawate, Nathan Merrill, Angel Qin, Sofia D. Merajver, Sunitha Nagrath, and Xudong Fan. Antigen-independent single-cell circulating tumor cell detection using deep-learning-assisted biolasers. *Biosensors and Bioelectronics*, 271:116984, 2025.
- [11] Ling An, Yi Liu, and Yaling Liu. Advancements in Circulating Tumor Cell Detection for Early Cancer Diagnosis: An Integration of Machine Learning Algorithms with Microfluidic Technologies. *Biosensors*, 15(4):220, 2025.
- [12] Istiak Ahmad and Fahad Alqurashi. Early cancer detection using deep learning and medical imaging: A survey. *Critical Reviews in Oncology/Hematology*, 204:104528, 2024.

- [13] Cheng Shen, Siddarth Rawal, Rebecca Brown, Haowen Zhou, Ashutosh Agarwal, Mark A Watson, Richard J Cote, and Changhui Yang. Automatic detection of circulating tumor cells and cancer associated fibroblasts using deep learning. *Scientific Reports*, 13(1):5708, 2023.
- [14] Ehsan Alizadeh, John Castle, Amanda Quirk, Christopher D L Taylor, Wei Xu, and Abhinav Prasad. Cellular morphological features are predictive markers of cancer cell state. *Computers in Biology and Medicine*, 126:104044, 2020.
- [15] Sayan Basu, Soheil Kolouri, and Gustavo K Rohde. Detecting and visualizing cell phenotype differences from microscopy images using transport-based morphometry. *Proceedings of the National Academy of Sciences*, 111(9):3448–3453, 2014.
- [16] Zhaozheng Yin, Takeo Kanade, and Mei Chen. Understanding the phase contrast optics to restore artifact-free microscopy images for segmentation. *Medical Image Analysis*, 16(5):1047–1062, 2012.
- [17] Carsen Stringer, Tim Wang, Michalis Michaelos, and Marius Pachitariu. Cellpose: a generalist algorithm for cellular segmentation. *Nature methods*, 18(1):100–106, 2021.
- [18] Jun Ma, Ronald Xie, Shamini Ayyadhury, Cheng Ge, Anubha Gupta, Ritu Gupta, Song Gu, Yao Zhang, Gihun Lee, Joonkee Kim, et al. The multimodality cell segmentation challenge: toward universal solutions. *Nature methods*, pages 1–11, 2024.
- [19] Christoffer Edlund, Timothy R Jackson, Nabeel Khalid, Nicola Bevan, Timothy Dale, Andreas Dengel, Sheraz Ahmed, Johan Trygg, and Rickard Sjögren. Livecell—a large-scale dataset for label-free live cell segmentation. *Nature methods*, 18(9):1038–1045, 2021.
- [20] Noah F Greenwald, Geneva Miller, Erick Moen, Alex Kong, Adam Kagel, Thomas Dougherty, Christine Camacho Fullaway, Brianna J McIntosh, Ke Xuan Leow, Morgan Sarah Schwartz, et al. Whole-cell segmentation of tissue images with human-level performance using large-scale data annotation and deep learning. *Nature biotechnology*, 40(4):555–565, 2022.
- [21] Kevin J Cutler, Carsen Stringer, Teresa W Lo, Luca Rappez, Nicholas Stroustrup, S Brook Peterson, Paul A Wiggins, and Joseph D Mougous. Omnipose: a high-precision morphology-independent solution for bacterial cell segmentation. *Nature methods*, 19(11):1438–1448, 2022.
- [22] Juan C Caicedo, Allen Goodman, Kyle W Karhohs, Beth A Cimini, Jeanelle Ackerman, Marzieh Haghighi, CherKeng Heng, Tim Becker, Minh Doan, Claire McQuin, et al. Nucleus segmentation across imaging experiments: the 2018 data science bowl. *Nature methods*, 16(12):1247–1253, 2019.
- [23] Gihun Lee, SangMook Kim, Joonkee Kim, and Se-Young Yun. Mediar: Harmony of data-centric and model-centric for multi-modality microscopy. *arXiv preprint arXiv:2212.03465*, 2022.
- [24] Jun Ma, Yuting He, Feifei Li, Lin Han, Chenyu You, and Bo Wang. Segment anything in medical images. *Nature Communications*, 15(1):654, 2024.

- [25] Olaf Ronneberger, Philipp Fischer, and Thomas Brox. U-net: Convolutional networks for biomedical image segmentation. In Nassir Navab, Joachim Hornegger, William M. Wells, and Alejandro F. Frangi, editors, *Medical Image Computing and Computer-Assisted Intervention – MICCAI 2015*, pages 234–241, Cham, 2015. Springer International Publishing.
- [26] Carsen Stringer and Marius Pachitariu. Cellpose3: one-click image restoration for improved cellular segmentation. *Nature Methods*, pages 1–8, 2025.
- [27] Tongle Fan, Guanglei Wang, Yan Li, and Hongrui Wang. Ma-net: A multi-scale attention network for liver and tumor segmentation. *IEEE Access*, 8:179656–179665, 2020.
- [28] Jun Ma and Bo Wang. Towards foundation models of biological image segmentation. *Nature Methods*, 20(7):953–955, 2023.
- [29] Uriah Israel, Markus Marks, Rohit Dilip, Qilin Li, Changhua Yu, Emily Laubscher, Shenyi Li, Morgan Schwartz, Elora Pradhan, Ada Ates, et al. A foundation model for cell segmentation. *bioRxiv*, pages 2023–11, 2024.
- [30] Marius Pachitariu and Carsen Stringer. Cellpose 2.0: how to train your own model. *Nature methods*, 19(12):1634–1641, 2022.
- [31] Anwai Archit, Luca Freckmann, Sushmita Nair, Nabeel Khalid, Paul Hilt, Vikas Rajashekar, Marei Freitag, Carolin Teuber, Genevieve Buckley, Sebastian von Haaren, et al. Segment anything for microscopy. *Nature Methods*, pages 1–13, 2025.
- [32] Peilin Zhou, Bo Du, and Yongchao Xu. Cellseg1: Robust cell segmentation with one training image. *arXiv preprint arXiv:2412.01410*, 2024.
- [33] Alexander Kirillov, Eric Mintun, Nikhila Ravi, Hanzi Mao, Chloe Rolland, Laura Gustafson, Tete Xiao, Spencer Whitehead, Alexander C Berg, Wan-Yen Lo, et al. Segment anything. In *Proceedings of the IEEE/CVF International Conference on Computer Vision*, pages 4015–4026, 2023.
- [34] Dimitrios Giakoumettis, Aristotelis Kritis, and Nikolaos Foroglou. C6 cell line: the gold standard in glioma research. *Hippokratia*, 22(3):105–112, 2018.
- [35] Joana Sarah Grah, Jennifer Alison Harrington, Siang Boon Koh, Jeremy Andrew Pike, Alexander Schreiner, Martin Burger, Carola-Bibiane Schönlieb, and Stefanie Reichelt. Mathematical imaging methods for mitosis analysis in live-cell phase contrast microscopy. *Methods*, 115:91–99, 2017.
- [36] Ultralytics. YOLOv11: Real-Time Object Detection. Available at: <https://github.com/ultralytics/ultralytics>, accessed 2025-03-07, 2024.
- [37] Anish Viridi and Ajit P Joglekar. Cell-APP: A generalizable method for microscopic cell annotation, segmentation, and classification. *bioRxiv*, 2025.
- [38] Binghao Chai, Christoforos Efstathiou, Haoran Yue, and Viji M Draviam. Opportunities and challenges for deep learning in cell dynamics research. *Trends in Cell Biology*, 34(11):955–967, 2024.

- [39] Clotilde Cadart, Ewa Zlotek-Zlotkiewicz, Maël Le Berre, Matthieu Piel, and Helen K Matthews. Exploring the function of cell shape and size during mitosis. *Developmental Cell*, 29(2):159–169, 2014.
- [40] Jonathan Flores et al. Automate nuclei detection using neural networks. *SMU Data Science Review*, 2(1):8, 2019.
- [41] Bin Xiao, Yunfeng Pan, and Xingpeng Zhang. DA-UNet: Deformable Attention U-Net for Nucleus Segmentation. In *Proceedings of the 2023 International Conference on Computer, Vision and Intelligent Technology (ICCVIT '23)*, pages 1–5. ACM, 2023.
- [42] A. Singha and M.K. Bhowmik. AlexSegNet: an accurate nuclei segmentation deep learning model in microscopic images for diagnosis of cancer. *Multimedia Tools and Applications*, 82:20431–20452, 2023.
- [43] D.-P. Tran, Q.-A. Nguyen, V.-T. Pham, and T.-T. Tran. Trans2Unet: Neural fusion for Nuclei Semantic Segmentation. In *2022 11th International Conference on Control, Automation and Information Sciences (ICCAIS)*, pages 583–588, 2022.
- [44] N.-M. Le, D.-H. Le, V.-T. Pham, and T.-T. Tran. DR-Unet: Rethinking the ResUnet++ Architecture with Dual ResPath skip connection for Nuclei segmentation. In *2021 8th NAFOSTED Conference on Information and Computer Science (NICS)*, pages 194–198, 2021.
- [45] P. Manju, B. R. Devassy, V. Rajan, and G. R. Gnana King. A Novel Approach for Nuclei Segmentation Using U-Net. In *2023 International Conference on Networking and Communications (ICNWC)*, pages 1–6, 2023.
- [46] N. Khalid, M. Caroprese, G. Lovell, J. Trygg, A. Dengel, and S. Ahmed. CellSpot: Deep Learning-Based Efficient Cell Center Detection in Microscopic Images. In *Artificial Neural Networks and Machine Learning – ICANN 2024*, M. Wand et al. (eds.), Lecture Notes in Computer Science, vol. 15023, Springer, Cham, 2024.
- [47] A. S. Raj, S. B. Asha, and G. Gopakumar. Feature Enhanced Semi-Supervised Attention U-Net for Cell Segmentation. In *2024 15th International Conference on Computing Communication and Networking Technologies (ICCCNT)*, pages 1–6, 2024.
- [48] Yating Zhou, Wenjing Li, and Ge Yang. SCTS: Instance Segmentation of Single Cells Using a Transformer-Based Semantic-Aware Approach. In *Proceedings of the IEEE/CVF Winter Conference on Applications of Computer Vision (WACV)*, pages 5944–5953, 2023.
- [49] N. Khalid et al. PACE: Point Annotation-Based Cell Segmentation for Efficient Microscopic Image Analysis. In *Artificial Neural Networks and Machine Learning – ICANN 2023*, L. Iliadis et al. (eds.), Lecture Notes in Computer Science, vol. 14255, Springer, Cham, 2023.
- [50] Clément Cazorla et al. Sketchpose: Learning to Segment Cells with Partial Annotations. *Machine Learning for Biomedical Imaging*, 3(August):367–381, 2025.

- [51] Wei Lou, Xinyi Yu, Chenyu Liu, Xiang Wan, Guanbin Li, Siqi Liu, and Haofeng Li. Multi-stream Cell Segmentation with Low-level Cues for Multi-modality Images. *Proceedings of The Cell Segmentation Challenge in Multi-modality High-Resolution Microscopy Images*, 212:1–10, 2023.

A Additional metrics without overlap

In Table 2, the metrics were computed under the assumption that object instances may overlap. By contrast, the evaluation in Table 4 was performed on non-overlapping masks, where all conflicts between instances were resolved deterministically using the same procedure that was applied during training for both MediarFormer and CellPose.

As can be seen from the table, all conclusions drawn from Table 2 remain valid. Notably, the lower metrics reported in Table 4 indicate potential for further improvement in MediarFormer and CellPose, particularly if their architectures are modified to accommodate overlapping cells.

Table 2: Glioma C6-spec performance comparison of cell segmentation models across different categories and subsets.

Model	Glioma-ft	Prec.	Rec.	F ₁	AP@50	AP@75	AP@90
Cells (both types), spec							
MediarFormer	✗	57.53	2.06	3.98	2.03	0.62	0.0
CellPose	✗	21.1	11.11	14.55	7.85	1.3	0.0
YOLOv11	✓	70.16	78.23	73.98	58.7	11.27	0.05
CellSeg1	✓	79.15	79.66	79.4	65.84	19.42	0.99
MediarFormer	✓	89.32	76.86	82.62	70.39	23.45	1.53
CellPose	✓	88.87	78.87	83.57	71.78	26.31	1.29
Soma, spec							
CellPose-nuclei	✗	0.43	0.31	0.36	0.18	0.03	0.0
YOLOv11	✓	77.29	77.14	77.21	62.89	4.25	0.0
CellSeg1	✓	83.52	82.15	82.83	70.69	25.0	0.49
MediarFormer	✓	89.4	85.88	87.61	77.95	32.99	0.87
CellPose	✓	88.15	87.11	87.63	77.98	32.68	1.25
CellPose-nuclei	✓	87.76	87.76	87.76	78.19	32.87	1.28
Cells type A, spec							
YOLOv11	✓	71.39	56.69	63.2	46.19	15.12	1.2
CellSeg1	✓	44.57	75.8	56.13	39.02	13.27	0.55
MediarFormer	✓	51.41	65.61	57.65	40.5	6.67	0.0
CellPose	✓	72.43	65.82	68.97	52.63	18.45	1.12
Cells type B, spec							
YOLOv11	✓	57.04	70.46	63.04	46.03	8.34	0.06
CellSeg1	✓	72.31	69.31	70.78	54.78	16.77	0.99
MediarFormer	✓	85.26	59.53	70.11	53.97	16.34	1.45
CellPose	✓	82.19	67.26	73.98	58.71	18.85	1.14
Cells, gen							
MediarFormer	✗	85.43	20.92	33.6	20.19	9.06	1.01
CellPose	✗	30.81	29.08	29.92	17.59	5.26	0.41
YOLOv11	✓	53.89	69.96	60.88	43.77	4.71	0.03
CellSeg1	✓	66.17	81.08	72.87	57.32	23.36	2.06
MediarFormer	✓	83.29	77.64	80.41	67.24	26.4	1.45
CellPose	✓	82.63	79.08	80.82	67.81	24.78	1.0

Table 3: Assessment of annotation uncertainty in the Glioma C6 dataset via comparison with independent expert annotations. Three experts independently re-annotated two test images, then produced a consensus annotation through discussion. The table reports the agreement between different annotation sources (original dataset annotation and CellPose predictions) and the expert consensus.

Annotation	AP@50		AP@75		AP@90	
	image 1	image 2	image 1	image 2	image 1	image 2
Cells (both types)						
Dataset annotation	0.7137	0.8117	0.1394	0.3478	0.0000	0.0072
CellPose	0.7445	0.8151	0.2073	0.4171	0.0051	0.0232
Soma						
Dataset annotation	0.7792	0.8514	0.2607	0.2925	0.0049	0.0000
CellPose	0.8739	0.8562	0.3419	0.3897	0.0146	0.0226
Cells type A						
Dataset annotation	0.6667	0.6744	0.0588	0.3091	0.0000	0.0000
CellPose	0.6170	0.7297	0.0704	0.3913	0.0000	0.0000
Cells type B						
Dataset annotation	0.6262	0.7395	0.1512	0.3185	0.0000	0.0098
CellPose	0.6062	0.7477	0.1969	0.2897	0.0065	0.0331

Table 4: **Glioma C6-spec performance comparison** of cell segmentation models across different categories and subsets without overlapping.

Model	Glioma-ft	Prec.	Rec.	F ₁	AP@50	AP@75	AP@90
Cells (both types), spec							
MediarFormer	✗	56.0	2.2	4.2	2.1	0.7	0.0
CellPose	✗	19.8	11.4	14.5	7.8	1.4	0.0
YOLOv11	✓	55.1	70.3	61.8	44.7	6.1	0.0
CellSeg1	✓	74.9	78.1	76.5	61.9	19.2	0.9
MediarFormer	✓	86.8	74.4	80.1	66.8	22.0	1.2
CellPose	✓	86.5	77.2	81.6	69.0	25.4	1.0
Soma, spec							
CellPose-nuclei	✗	0.5	0.4	0.4	0.2	0.0	0.0
YOLOv11	✓	74.0	76.0	75.0	60.0	4.3	0.0
CellSeg1	✓	82.8	81.1	81.9	69.4	22.2	0.3
MediarFormer	✓	89.3	84.6	86.9	76.9	32.8	0.7
CellPose	✓	89.0	86.9	87.9	78.5	33.9	1.4
CellPose-nuclei	✓	88.0	87.7	87.8	78.3	33.2	1.5
Cells type A, spec							
YOLOv11	✓	37.7	55.5	44.9	28.9	4.6	0.0
CellSeg1	✓	44.3	73.2	55.2	38.1	14.4	0.8
MediarFormer	✓	70.8	57.7	63.5	46.6	16.2	1.0
CellPose	✓	65.6	66.7	66.1	49.4	19.1	1.2
Cells type B, spec							
YOLOv11	✓	42.9	59.1	49.7	33.1	5.2	0.1
CellSeg1	✓	69.0	68.5	68.8	52.4	16.3	1.0
MediarFormer	✓	81.5	57.7	67.6	51.0	15.2	1.0
CellPose	✓	78.7	65.9	71.7	55.9	17.7	0.9
Cells, gen							
MediarFormer	✗	81.2	20.4	32.6	19.5	8.3	0.7
CellPose	✗	30.1	31.6	30.8	18.2	5.5	0.5
YOLOv11	✓	38.2	59.0	46.4	30.2	2.7	0.0
CellSeg1	✓	62.7	81.1	70.7	54.7	21.1	1.6
MediarFormer	✓	80.4	75.4	77.8	63.7	21.2	1.0
CellPose	✓	80.3	76.8	78.5	64.6	19.9	0.7